processes

MDPI

Article

Design and Performance Evaluation of Liquid-Cooled Heat Dissipation Structure for Lithium Battery Module

Yifei Zhao, Jianhong Chen * and Wanrong He

School of Resource and Safety Engineering, Central South University, Changsha 410083, China; zhaoyifei@csu.edu.cn (Y.Z.)
* Correspondence: jhchen@csu.edu.cn

Abstract: The current global resource shortage and environmental pollution are becoming increasingly serious, and the development of the new energy vehicle industry has become one of the important issues of the times. In this paper, a nickel–cobalt lithium manganate (NCM) battery for a pure electric vehicle is taken as the research object, a heat dissipation design simulation is carried out using COMSOL software, and a charging heat generation model of the battery pack is established. Combined with the related research on the thermal management technology of the lithium-ion battery, five liquid-cooled temperature control models are designed for thermal management, and their temperature control simulation and effect analysis are carried out. Finally, the performance evaluation system of the thermal management scheme of the lithium-ion battery pack is established based on the analytic network process (ANP) and system dynamics (SD), and the performance of the above five thermal management design models is comprehensively scored and analyzed. The results show that liquid-cooled Models 1 (86.7075) and 5 (89.1055) have the highest overall scores, meeting both the temperature control requirements and the overall thermal management performance, and it is recommended to apply the working condition settings for which they are evaluated as Level *I*.

Keywords: NCM battery; thermal management scheme; liquid cooling heat dissipation; analytic network process; system dynamics

Citation: Zhao, Y.; Chen, J.; He, W. Design and Performance Evaluation of Liquid-Cooled Heat Dissipation Structure for Lithium Battery Module. *Processes* **2023**, *11*, 1769. https://doi.org/10.3390/pr11061769

Academic Editors: Jilei Ye and Zhuoyuan Zheng

Received: 17 May 2023
Revised: 27 May 2023
Accepted: 2 June 2023
Published: 10 June 2023

1. Introduction

Lithium-ion batteries have become the most widely used energy source for electric vehicles due to advantages such as their smaller volume and weight, larger storage capacity, better cycle performance, and environmental friendliness. However, they have also become a power source of concern in academic research. Currently, most pure electric vehicles on the market adopt lithium nickel cobalt manganese oxide batteries and lithium iron phosphate batteries, and the most mature process is cylindrical cells. The key to the development of pure electric vehicles lies in the thermal safety of their lithium-ion battery packs [1–4]. Their performance is easily affected by overheating, overcharging, short circuits, impacts, and other factors, which can shorten the life of the battery pack and greatly reduce the cruising range [5–7]. According to the statistics, from 2017 to 2020 alone, China had 54 spontaneous combustion accidents involving pure electric vehicles, causing direct economic losses of about CNY 145.181 million. However, Nelson et al. found that rapidly heating the battery pack to reach the effective temperature range is more difficult than dissipating the heat generated by the battery because a moderate temperature rise within a proper range is beneficial to the battery [8]. However, a sharp uncontrolled increase in the temperature of the battery pack will also accelerate the chemical reaction process, causing corrosion and damage to the battery materials and components, leading to premature battery failure or even triggering a series of thermal runaway safety incidents [9]. Therefore, designing a thermal management solution to keep the battery within a suitable temperature range for a long time and reduce the temperature difference between regions

as much as possible to maintain the overall uniformity of temperature is the key to the problem [10–12]. Existing lithium-ion battery thermal management technologies mainly include air cooling, liquid cooling, phase change materials (PCMs), and combinations of the above two or more forms [9–11,13–15].

The principle of air cooling heat dissipation is to generate cold and hot air flow through ambient air, self-provided equipment, or external auxiliary equipment, such as fans, to achieve convective heat transfer from the battery pack [16,17]. Pesaran and Park optimized the gas flow path through simulation, and the optimized air cooling method can keep the battery pack within a certain interval [18,19]. Nelson et al. found that the low thermal conductivity of air cannot achieve rapid cooling in high-temperature environments and must be combined with other thermal management methods to meet the requirements [8]. Wang et al. proposed a new method to improve the cooling performance of BTMSs. The parallel plate mounting method can effectively improve the air flow distribution of the battery pack and effectively improve the cooling efficiency of BTMSs [20].

Liquid cooling uses a coolant as a medium for convective heat transfer to achieve heat dissipation and cooling of the battery pack through direct or indirect contact [21]. Currently, the related research focuses on the shape of liquid cooling channels, the optimization of the cooling structures, and the selection of the coolant materials [22]. Chen, Dafen et al. compared air cooling, contact liquid cooling, and noncontact liquid cooling and believed that noncontact liquid cooling has the best thermal performance [23]. Wu M et al. believe that compared with straight tubes and U-shaped pipes, the wavy structure has a better heat dissipation effect [24]. Gao et al. developed a BTMS design based on the along-flow gradient channel and applied it to cylindrical lithium-ion battery modules. Compared with the uniform channel design, the gradient channel design (GCD) significantly changed the basic characteristic of the monotonically increasing temperature along the flow direction. Optimizing the number of line segments and segment length combinations, the optimal GCD significantly enhanced thermal uniformity over the entire flow range [25]. The application of liquid cooling also has problems, such as leakage and heat conduction, which greatly affects the overall effect of temperature control and leads to a significant increase in cost [26].

For phase change materials, experts have studied various composite PCM systems for the low thermal conductivity of paraffin [27,28]. Mainly expanded graphite (EG) [29–31], metal materials (aluminum foam [32] and copper foam [33]), carbon fiber [34] or carbon nanotubes [35], and paraffin are used to prepare composite PCMs to improve the overall performance of the PCMs. A PCM can be in direct contact with the battery without consuming external energy. While cooling, it can achieve an insulation effect, meeting the requirements of vehicle weight reduction. It occupies less space than the air cooling and liquid cooling of the battery pack. However, it also has disadvantages, such as low thermal conductivity, slow heat storage, and possible segregation [36,37].

In summary, the selection of the battery thermal management means needs to be reselected according to the different heat generation situations during battery charging to then establish a battery charging heat generation model as the basis for selecting the thermal management means.

2. Modeling and Simulation of Battery Pack Charging Heat Generation Conditions

2.1. Heat Generation Mechanism and Heat Transfer Mechanism of Lithium Batteries

The heat generation mechanism of lithium-ion batteries is mainly due to the working principle and characteristics of the lithium-ion battery; the working process is always accompanied by the occurrence of various reaction processes inside it, which leads to a large amount of heat generation and accumulation inside it. Therefore, the heat generation source of the battery unit is mainly composed of Joule heat Qj generated by overcoming the work of resistance, reaction heat Qr generated during normal operation, polarization heat Qp generated by electrode imbalance, and heat generation Qf in the secondary reaction stage of the battery.

Among them, the side reactions that generate heat Qf mainly include SEI film decomposition reaction, negative electrode and electrolyte reaction, positive electrode and

electrolyte reaction, and electrolyte decomposition. These reactions not only damage the battery material but also produce some gases in the process, causing the battery to swell the pack, thus further damaging the battery structure and affecting the battery performance, causing irreversible damage to the battery.

The battery heat in overcharge mainly comes from two major parts: *Qj* and *Qf*. In addition, as the temperature inside the battery increases, more side reactions are excited, and heat is released, resulting in thermal runaway as the heat release rate of the battery accelerates with the increase in temperature.

The heat transfer mechanism of the lithium-ion battery mainly consists of three aspects: heat conduction, heat convection, and heat radiation. In this paper, we ignore the heat conduction and heat radiation inside the battery pack and consider only the natural convection between the battery pack and the environment in the simulation of the battery pack thermal model, but we consider all three heat transfer mechanisms in the subsequent simulation of the thermal design scheme.

2.2. Numerical Model

The simulation object of this model is an 18,650 NCM battery used in a pure electric vehicle, and according to the introduction and records of the battery in the power battery technology agreement provided by the pure electric vehicle, the main component materials and some parameters of the battery unit are summarized in Table 1. A 5 × 5 scale 18,650-type NCM matrix battery pack model was established with external 120 mm × 120 mm × 70 mm external wall (Figure 1a). Each cell was simplified to a cylinder with a radius of 9 mm and a height of 65 mm (ignoring features such as protruding electrodes on the cell), and the whole cell was arranged with equal spacing (adjacent to the cell circle distance) of L = 24 mm. Before meshing, the geometric model needed to be processed accordingly to ensure smooth meshing. A total of 293,462 grid cells were generated in the mesh division, and the average cell mass was 0.6461. The comprehensive division results are reasonable and can be seen in Figure 1b,c. In terms of the values of the thermal property parameters of the NCM cell monomer, this paper summarizes and compiles a table of the thermal property parameters of the main components of the NCM cell monomer by integrating the relevant settings of these parameters from some related literature [38–40], which is shown in Table 2.

Table 1. Specifications and parameters of the NCM battery.

Specification	Value	Specification	Value
Model	18,650~2.6 Ah	Charging temperature (°C)	0~50
Monomeric mass (kg)	0.046	Discharge temperature (°C)	−20~60
Standard voltage (V)	3.7	Rated input current (A)	0.86
Voltage range (V)	2.7~4.2	Electrolyte material	LiPF6
Internal resistance (mΩ)	4	Anode material	$LixC_6$
Number of cycles	1000	Cathode material	$LiNi_{1/3}Mn_{1/3}Co_{1/3}O_2$
Specification	Value	Specification	Value

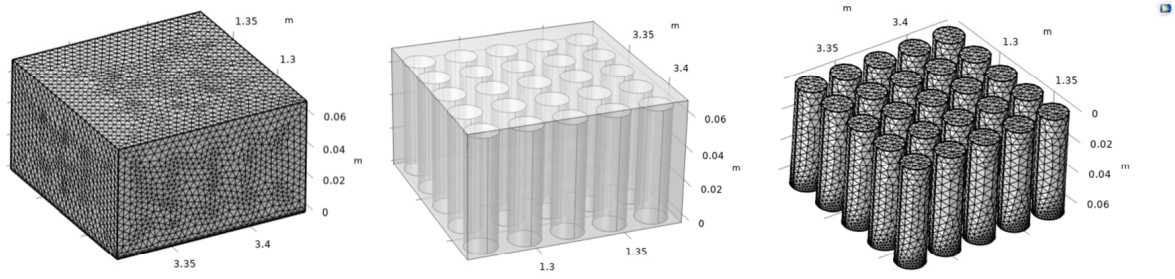

(a) Geometric model **(b) Housing grid** **(c) Battery pack grid**

Figure 1. Geometric modeling and meshing of NCM battery pack.

Table 2. Thermal and physical parameters of the NCM battery.

Battery Material	Thermal Conductivity (W/(m·K))	Density (kg/m^3)	Specific Heat Capacity (J/(kg·K))
Copper foil	398	8900	385
Cathode	1.5	2380	710
Diaphragm	0.334	1009	1978
Anode	1.04	2660	1437.4
Aluminum foil	238	1500	903
Electrolyte	0.6	1130	2055
Stainless steel case	44.5	460	7800

2.3. Boundary Conditions

1. The geometric model ignores the actual situation inside the NCM cell monolith and simplifies the cell monolith to a cylinder uniformly;
2. The heat of polarization, heat of reaction, and reversible heat of the cell are not considered, and only the joule heat and side reaction exotherm of the cell are used as the heat sources inside the cell;
3. For the NCM battery pack charging thermal model, the boundary conditions only consider natural thermal convection. Subsequent thermal management design simulations also consider heat conduction and heat radiation;
4. The thermal conductivity of each individual cell is a constant, and its variation with the outside world is ignored;
5. The temperature thresholds are set to simulate the side reaction process: at 90 °C < T < 120 °C, the SEI film decomposes; at T > 120 °C, the negative electrode reacts; at T > 170 °C, the positive electrode reacts; and at T > 200 °C, the electrolyte reacts;
6. No gas is produced in the model during the simulation, i.e., no gas phase is generated, and the volume expansion of the NCM cell monomer and the change of internal stress brought about during the reaction are ignored.

2.4. Simulation Results and Analysis

2.4.1. Simulation and Analysis of Overcharge of NCM Battery Pack under Different Charging Multiplier Conditions

The initial temperature and ambient temperature of the NCM battery pack were set to 293.15 K (20 °C), the natural convection coefficient was 7.17 W/(m^2·K), and the inlet wind speed was 1 m/s. On this basis, the charging and exothermic simulation of the battery pack under the charging multiplier of 0.3 C, 0.5 C, 0.8 C, and 1 C working conditions were simulated, respectively, and the model simulation was carried out according to the parameters in the table. According to the relevant studies, it is confirmed that the maximum temperature and temperature uniformity are two important criteria to evaluate the performance of thermal management systems [41]. Therefore, the subsequent simulation analysis focused on the maximum temperature and temperature uniformity.

The maximum temperature rise data curves of the battery pack under the four operating conditions are summarized and plotted in Figure 2a, and the following analysis was obtained:

1. Under the 0.3 C condition, the battery pack did not experience thermal runaway of charging, the charging current was 0.78 A, and the overall temperature remained between 20 and 26.1 °C, reaching the maximum temperature (26.1 °C) at about 5250 s, and the overall temperature rise was slow. The accumulation of Joule heat did not reach 90 °C during the whole charging simulation time (30,000 s) to trigger the subsequent corresponding side reaction process. The thermal simulation image of the battery surface temperature at full charge (12,000 s) was intercepted (Figure 2b). From the figure, the battery temperature rise meets the technical requirements of the safety range (0~50 °C), and the maximum temperature difference between the groups is also small at only 4.3 °C. Such a temperature difference is common inside the lithium-ion battery pack, which brings certain safety risks to the battery pack;

2. Under the 0.5 C operating condition, the maximum temperature of the battery pack exceeded the charging safety temperature threshold of 50.4 °C at about 1700 s and remained above 61 °C until the end of charging (7200 s), which is beyond the safety temperature range and means that the battery may fail at a high temperature for individual cells. Although the battery pack at the charging current of 1.3 A did not occur charging thermal runaway, compared to the 0.3 C operating conditions, the overall temperature at this time to be maintained between 20 and 62 °C almost doubled the temperature rise at 0.3 C; the rate of warming was also significantly increased, and the benefit is to shorten the charging time of 4800 s. The interception of fully charged moment (7200 s) of the battery surface temperature is shown in the simulation image (Figure 2c). It can be seen from the figure that the maximum temperature difference between the battery pack units reaches 34.1 °C at this time, and the temperature between the groups is extremely uneven, which is extremely damaging to individual cells and may affect the performance of the battery pack or even trigger a short circuit within the battery pack;
3. In the 0.5 C working condition, battery pack thermal runaway occurred; the maximum temperature of the battery pack under this condition even exceeded 550 °C, and the side reaction process occurred more rapidly, and the temperature fell back to about 214 °C again in the late reaction. The images of the battery pack reaching near to 90 °C (1590 s) (Figure 2d) and the thermal simulation images of the battery surface at full charge (4500 s) (Figure 2e) were intercepted. The battery triggers the decomposition reaction of the SEI film, which rapidly accumulates a large amount of heat and continues to trigger other side reaction processes, and finally, the thermal runaway phenomenon occurs, and the charging current under this condition is 2.08 A, which shows that the danger of high-current fast charging is great. Therefore, users should not use high-power mismatched charging equipment to charge pure electric vehicles without authorization;
4. Under the 1.0 C working condition, the battery pack side reaction was more intense, which made more battery units trigger thermal runaway one after another in a shorter period, resulting in the highest internal temperature curve of the battery pack in a shorter period with repeated agitation, which dropped back to the level of about 320 °C in the late reaction stabilization. The images of the battery pack reaching near to 90 °C (1550 s) (Figure 2f) and the thermal simulation images of the battery surface at full charge (3600 s) (Figure 2g) were intercepted. As can be seen, the charging current at this condition is 2.08 A, and the NCM monomer triggers a side reaction shortly after 1550 s, which is less than half the time required for a full charge. In addition to the four corners of the battery pack air flow rate being faster, the battery monomer can still maintain a relatively stable state; at this time, the whole box of the battery pack should have already burned or even exploded.

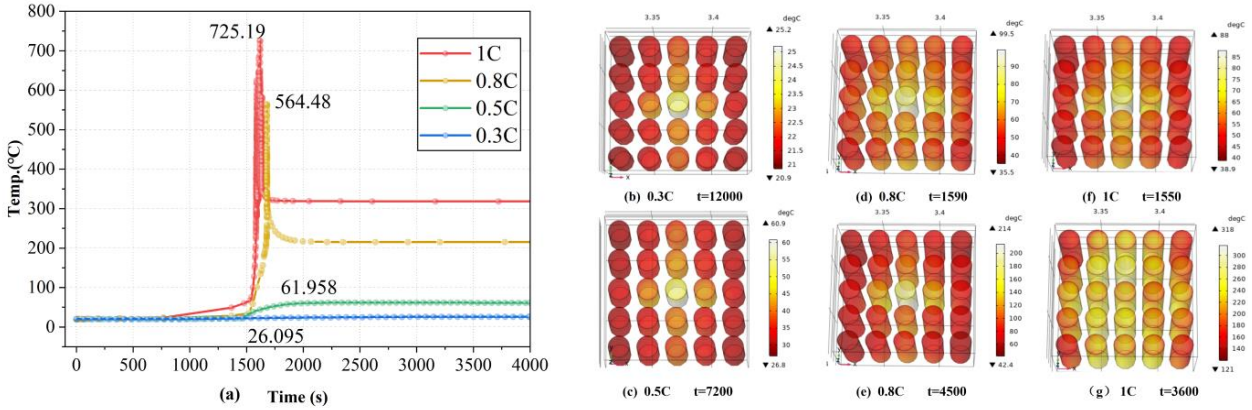

Figure 2. Thermal simulation images of the maximum temperature rise curve and surface temperature of NCM battery pack under different working conditions.

A comprehensive analysis of the performance of the conditions and the rated input current of this model NCM battery cell at 0.86 A in the subsequent thermal simulation will be carried out under the 0.5 C (1.3 A, 7200 s) charging multiplier condition.

2.4.2. Simulation and Analysis of NCM Battery Pack Overcharge under Different Ambient Temperature Conditions

The charging multiplier of the NCM battery pack was selected as 0.5 C (1.3 A, 7200 s), and the charging exotherm was simulated at 250, 30 °C, and 35 °C, respectively, and compared with the simulated 20 °C operating conditions. The maximum internal temperature of the battery pack with the charging time is shown in Figure 3a, and the thermal simulation images of the surface temperature of the NCM battery pack at full charge (7200 s) under these ambient temperature conditions were captured, respectively (Figure 3b–d). It can be seen from Figure 3 that the influence of the ambient temperature on the maximum temperature rise of the battery pack under this condition is linearly superimposed, but its influence is not negligible and still requires a more flexible response from the thermal management system to set the appropriate temperature control parameters in different seasons.

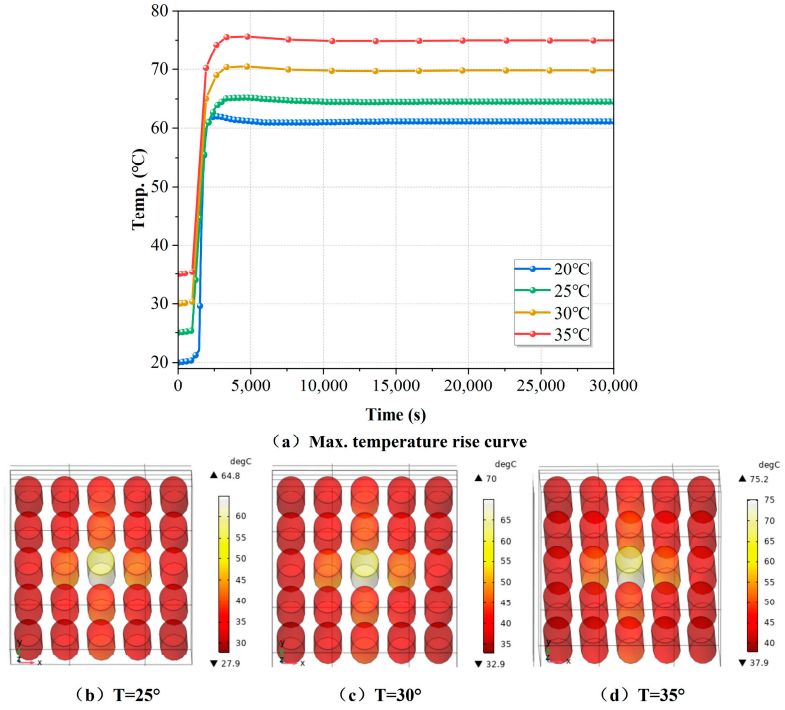

Figure 3. Thermal simulation images of the maximum temperature rise curve and surface temperature of NCM battery pack at different ambient temperatures.

3. Analysis of Battery Pack Thermal Management Technology

Currently, there are three main mainstream thermal management tools: air cooling [8,16–20,42], liquid cooling [21–26], and phase change materials (PCMs) [29,30,32,33,35–37,43]. The main components include fan forced convection cooling, air conditioning cooling, cold tube heat exchange liquid cooling, cold plate heat exchange liquid cooling, and phase change material temperature control techniques. The characteristics, advantages, and disadvantages related to the thermal management performance of these thermal management techniques are summarized using the literature research (Tables 3 and 4). The thermal management method of PCMs must be used in combination with other temperature control techniques because of its low thermal conductivity and the amount of latent heat of phase change required to achieve a certain amount. However, its high investment is not economical enough for thermal management systems, so the temperature control design of PCMs is not used in this paper. For the thermal performance of the NCM battery pack, the liquid

cooling method of cold plate heat exchange was selected to design the thermal control system for the NCM battery pack heat dissipation.

Table 3. Characteristics of various thermal management techniques.

Thermal Management Technology		Air-Cooled		Liquid Cooling		Phase Change Material
		Fan Cooling	Air Conditioning Cooling	Cold Tube Cooling	Cold Plate Cooling	
Cooling effect	Contrast room temp.	Higher	Lower	Lower	Lower	Higher
	Range	Controlled	Controlled	Controlled	Controlled	Wide
	Efficiency	Low	Moderate	High	High	Low
Environmental impact		Larger	Moderate	Smaller	Smaller	Larger
Temperature uniformity		Poor	Moderate	Better	Better	Good
Useful life		≥20 years	3 to 5 years	≥20 years	≥20 years	≥20 years
Difficulty of maintenance		Easy	Moderate	Difficult	Moderate	Moderate
Difficulty of application		Easy	Easier	Moderate	Easier	Easier
First investment		Low	Moderate	High	Moderate	High
Daily investment		Low	Higher	Moderate	Moderate	Low

Table 4. Advantages and disadvantages of thermal management technology.

Cooling Mode	Advantages	Disadvantages
Air-cooled (Fan cooling)	Simple construction; lighter weight; removes harmful gases from the battery pack; no risk of leakage	Easy to introduce external dust or water vapor, which can cause moisture, poor contact, or even short-circuiting of the battery
Air-cooled (Air conditioning cooling)	Simple construction; lighter weight; removes harmful gases from the battery pack; no risk of leakage	Filtered air must be used
Liquid-cooled (Cold tube heat transfer)	Can be integrated into vehicle cooling systems; high heat transfer coefficient	Possibility of fluid leakage; relatively high weight
Liquid-cooled (Cold plate heat exchange)	Can be integrated into vehicle cooling systems; high heat transfer coefficient	Possibility of fluid leakage; relatively high weight
Phase Change Material	Can be used repeatedly; can be set in direct contact with the battery	Low thermal conductivity; needs to be combined with other thermal management techniques

4. Liquid Cooling Temperature Control Design and Numerical Simulation Analysis

4.1. Liquid-Cooled Thermal Management Temperature Control Solution Design

In the liquid cooling thermal management temperature control design, this paper uses serpentine cold plates as well as ring-shaped cold plates for the battery pack liquid cooling design; there are five types of liquid cooling plate models, as shown in Figure 4a.

As can be seen, Models 1, 2, and 3 are a purely serpentine cold plate design. The design idea is as follows: first, the battery pack is placed in a staggered arrangement (at this time, the distance between the adjacent batteries is still kept at 24 mm, the angle between the three batteries of Model 1 is 60°, and the angle between the three batteries of Models 2 and 3 is 120°), and then the horizontal and vertical serpentine liquid cooling tubes are arranged along the battery pack to obtain Models 1 and 2, while Model 3 is made by rotating the lower part of Model 2 by 90° and stacking the upper and lower parts; therefore, Model 3 is actually a liquid-cooled design with two serpentine tubes. Models 4 and 5 are different from the previous designs in that instead of the coolant flowing through one row of monoliths before flowing to the next, it flows to the center of the battery pack, which heats up faster and then extends to the surrounding monoliths. Model 4 is a circular wiring design, and Model 5 is in the battery pack matrix arrangement method, where the serpentine cold plate is arranged with pipes according to the arrangement idea of center

first and then around. In addition, the inlet and outlet of the coolant are both 6 mm wide and 65 mm high.

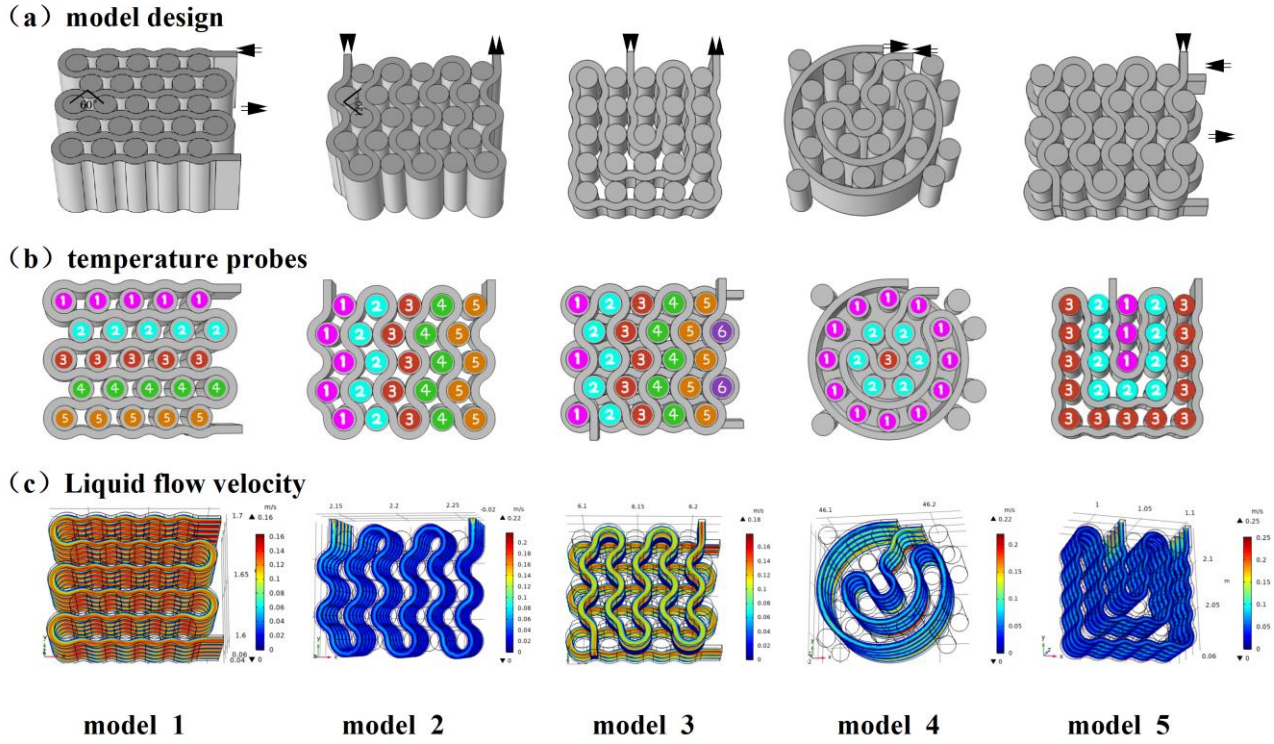

Figure 4. Liquid flow velocity distribution in the cold plate (xy direction cross-section).

4.2. Simulation and Analysis of Liquid-Cooled Temperature Control Model

4.2.1. Temperature Measurement Probe Arrangement

The arrangement of the temperature measurement probes was targeted according to the characteristics of the model, as shown in Figure 4b. The temperature measurement result was selected as the maximum temperature rise of one or more of the measured monomers at that moment. In the following simulations, the maximum temperature rise line was measured and plotted according to this probe arrangement.

4.2.2. Simulation and Analysis of Temperature Control of Each Liquid Cooling Model under Charge Multiplier of 0.5 C

The ambient temperature was set to 20 °C for all models, and the natural convection coefficient was 7.17 W/(m^2·K). Water was selected as the cooling fluid in the simulation and set as a fluid with a flow rate of 0.1 m/s and a temperature of 20 °C. The pressure at the wall of each model cold plate and the internal coolant flow are shown in Figure 4c. From the figure, we can see that the coolant flow rate is better in each model. Comparing Model 1 and Model 2, the cooling pipe envelope angle becomes larger, and the flow rate near the pipe wall decreases accordingly. Therefore, using the method of setting the cold plate with the center extending outward can make the coolant in the cold plate located near the center obtain a higher flow rate and thus carry away more heat. Comparing Model 3 with Models 1 and 2, Model 3 has a more uniform flow field by only reducing the pipe height by half. When looking at the flow velocity of the ring-shaped cold plate design, the ring-shaped design is much smoother than the serpentine cold plate, resulting in a more pronounced difference in the flow velocity between the upper and lower layers of the pipe, which may affect its thermal control effect.

On this basis, the simulation of charging the exotherm of Models 1~5 at the charging multiplier under the 0.5 C operating condition was carried out. According to the data of the temperature probe, the curves of the maximum internal temperature of the battery

pack of each model were plotted with time, which are shown in Figure 5a. As can be seen, Model 1, Model 2, and Model 5 have very good temperature uniformity under the 0.5 C working condition, and the temperature difference between the groups does not even exceed 1 °C, and the temperature difference of each row of individual cells in Model 1 and Model 2 is only about 0.2 °C. While observing the graphs of Model 3 and Model 4, it can be seen that the temperature difference of Model 4 has exceeded 12 °C, and although the temperature difference between the groups of Model 3 is not as large as that of Model 4, its overall temperature rise is the largest among all models, and there are large problems in both models. The thermal simulation images of the battery pack surface temperature at full charge (7200 s) in Models 1~4 were intercepted (Figure 5b). Observing the location of the higher temperature singlet in each model, they all appear in the fringe area or the area with larger voids in the cold plate. This is mainly because the temperature control of the liquid cooling plate mainly relies on the heat transfer via conduction between the contact surface of the cold plate and the monomer, the monomer at the edge of the cold plate, or the monomer in the model with a large gap; they all have a small contact area with the cold plate, which greatly affects the heat transfer efficiency of the cold plate. This is also the main reason for the large deterioration of the temperature uniformity between the groups of Model 3 and Model 4. The temperature control performance of each model in the full charge time under the statistical 0.5 C working condition is shown in the data in Table 5. Model 1, Model 2, and Model 5 are better cold plate designs, which can achieve better intergroup uniformity and temperature control.

Table 5. Temperature control data for each liquid cooling design from 0 s to 7200 s under 0.5 C charging condition.

Temperature Control Performance	Model 1	Model 2	Model 3	Model 4	Model 5
Temperature range (°C)	20~24.12	20~26.35	20~40.80	20~35.49	20~26.34
Temperature control effect (°C)	−37.88	−35.65	−21.20	−26.51	−35.66
Max. temperature difference (°C)	0.54	0.52	5.91	12.86	0.75
Occurrence of side-effects	NO	NO	NO	NO	NO

4.2.3. Simulation and Analysis of Temperature Control of Each Liquid Cooling Model under Different Coolant Flow Rate Conditions

Referring to the other literature on liquid-cooled designs, it is found that the more successful flow conditions are generally 0.2~0.7 m/s [33], so here, in this paper, the flow conditions of 0.3 m/s, 0.5 m/s, and 0.7 m/s were chosen to carry out the relevant studies on five liquid-cooled models and compare with the previous 0.1 m/s condition. The charge multiplier was chosen to be 0.5 C (1.3 A, 7200 s), and the other simulation conditions were kept constant. The variation curves of the maximum temperature inside the battery pack with the charging time for each liquid-cooled model at different flow rate conditions were plotted separately (Figure 6). As can be seen from the graphs, the battery pack temperature in each model decreases when the coolant flow rate rises to 0.3 m/s. However, there is no longer a significant cooling effect when the flow rate rises further, and several flow rate conditions of liquid-cooled Model 4 and Model 5 are even close to overlapping. Therefore, in the liquid-cooled thermal management system model, the temperature control effect that can be achieved only by increasing the coolant flow rate is limited, and the energy utilization efficiency will also decrease rapidly with the increasing flow rate. The temperature measurement data in the simulation were integrated, and the temperature control performance data of each model in the full charge time are plotted in Table 6.

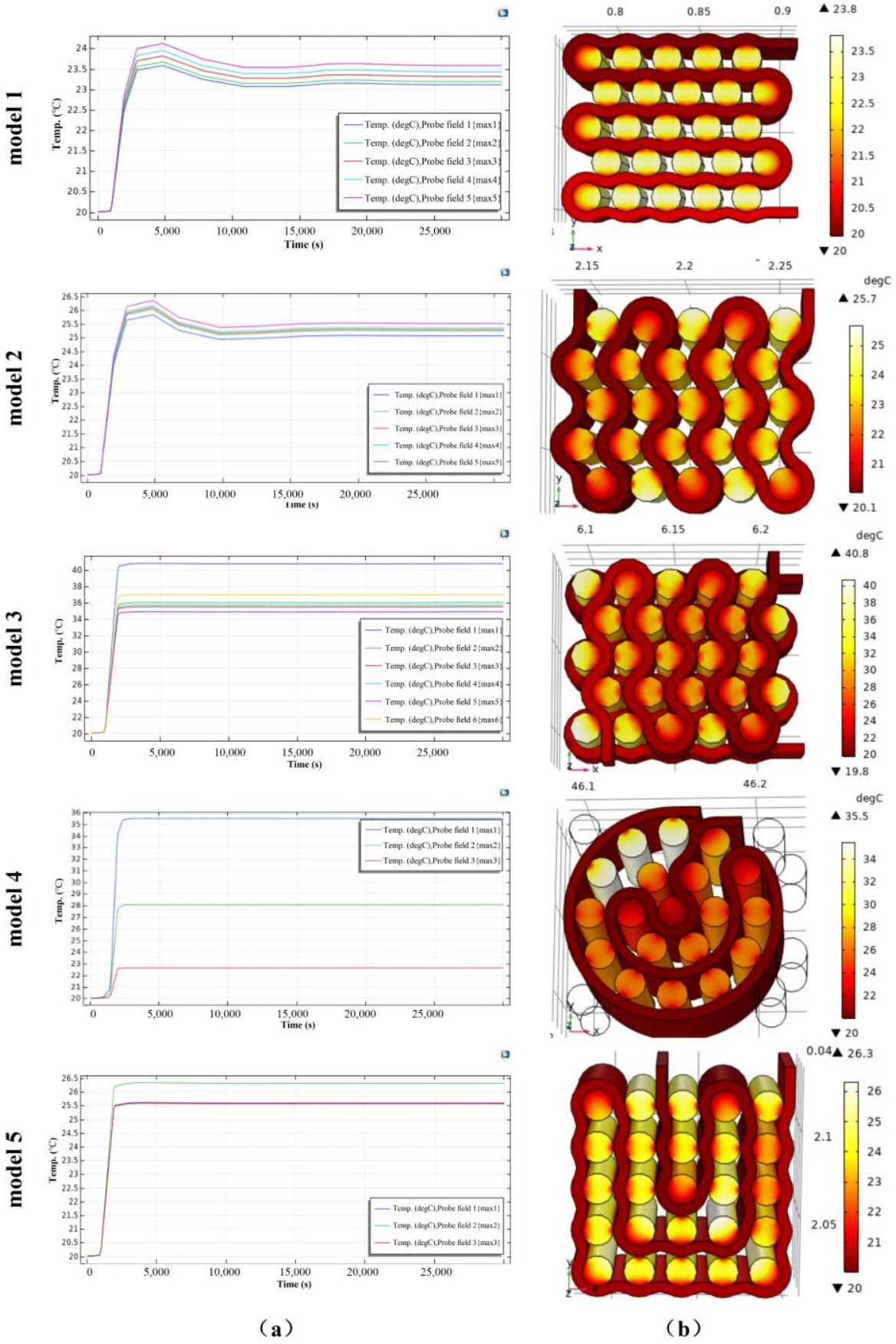

Figure 5. NCM battery pack liquid cooling temperature control maximum temperature rise curve (**a**) and surface temperature thermal simulation image (**b**).

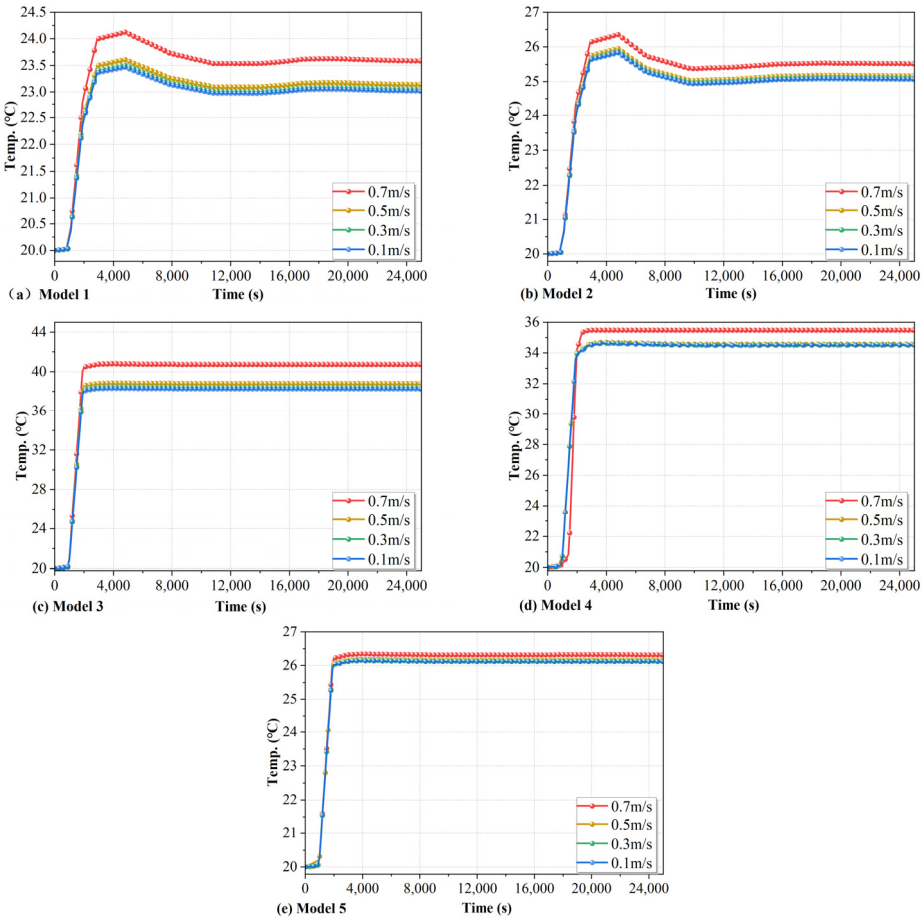

Figure 6. Max. temp. rise curves of NCM battery pack under different coolant flow rate working conditions.

Table 6. Temperature control data for each liquid cooling design from 0 s to 7200 s under different cooling liquid flow rate operating conditions.

Temperature Control Performance		Model 1	Model 2	Model 3	Model 4	Model 5
Flow rate (0.1 m/s)	Max. temp (°C)	24.12	26.35	40.80	35.49	26.34
	Max. temp difference (°C)	0.54	0.52	5.91	12.86	0.75
Flow rate (0.3 m/s)	Max. temp (°C)	23.61	25.95	38.86	34.70	26.18
	Max. temp difference (°C)	0.21	0.20	4.80	12.28	0.93
Flow rate (0.5 m/s)	Max. temp (°C)	23.51	25.87	38.47	34.64	26.15
	Max. temp difference (°C)	0.14	0.14	4.72	12.23	0.97
Flow rate (0.7 m/s)	Max. temp (°C)	23.47	25.84	38.30	34.62	26.13
	Max. temp difference (°C)	0.11	0.11	4.72	12.21	0.98

Under the working condition of 0.3 m/s, the maximum temperature rise of each model and the temperature difference between groups can meet the charging requirements of the NCM battery pack and achieve a better temperature control effect; in addition, the working condition of further increasing the flow rate obviously does not cause more decrease in the maximum temperature of each model, but, on the contrary, the temperature difference of Model 5 has a smaller increase. Based on the comprehensive analysis of the above, the following matching scheme of models and flow rates is preferred in this paper: a flow rate of 0.3 m/s was applied in Models 1, 2, 3, and 4, and a flow rate of 0.1 m/s was applied in Model 5.

4.2.4. Simulation and Analysis of Temperature Control of Each Liquid Cooling Model under Different Coolant Temperature Conditions

Combined with the above analysis for each flow rate working condition, the preferred model and flow rate matching scheme were used to further investigate the effect of the coolant temperature on battery pack heating in each model. The charge multiplier was chosen to be 0.5 C, and the charge exotherm was simulated at the temperature conditions of 19 °C, 18 °C, and 17 °C, respectively, and compared with the condition of 20 °C, while other simulation conditions were kept constant. The variation curves of the maximum temperature inside the battery pack with the charging time for each liquid-cooled model under different coolant temperature conditions were plotted (Figure 7). From the simulation and analysis of the temperature control of each liquid cooling model under different coolant temperature conditions, it can be seen that the effect of the coolant temperature on the overall temperature control of the model is linearly superimposed, which is a relatively easy factor for the overall model to adjust to achieve the temperature control goal. The temperature measurement data of each probe were combined, and the temperature control performance of each model during the full charge time is plotted in Table 7.

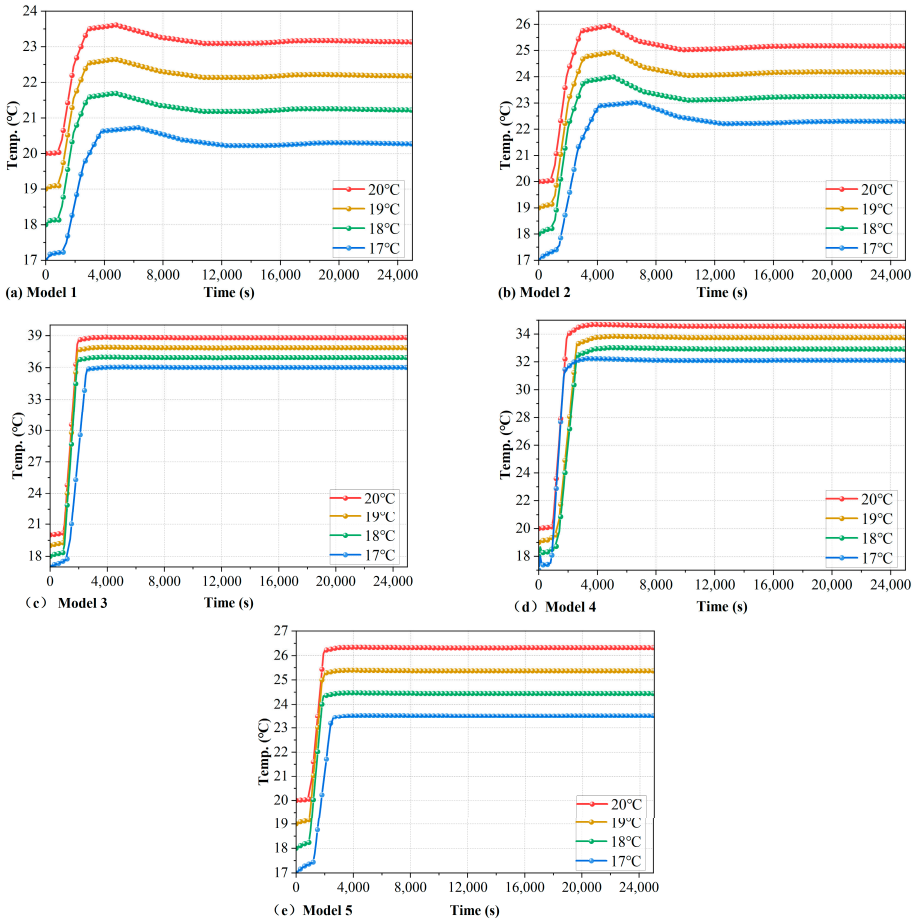

Figure 7. Max. temp. rise curves of NCM battery pack under different coolant temperature conditions.

Changing the coolant temperature can only linearly reduce the maximum temperature rise of the battery pack, but there is no improvement in the intergroup temperature difference or even a slight tendency to increase; the fluctuations are small and acceptable. Comparing the maximum temperature rise and maximum intergroup temperature difference of each model in the table, we can see that the temperature control effect of each model is roughly Model 1 ≈ Model 2 > Model 5 > Model 3 > Model 4.

Table 7. Temperature control data for each liquid-cooled design from 0 s to 7200 s under different cooling liquid temperature operating conditions.

Temperature Control Performance		Model 1	Model 2	Model 3	Model 4	Model 5
Temp. (20 °C)	Max. temp. (°C)	23.61	25.95	38.86	34.70	26.34
	Max. temp. difference (°C)	0.21	0.20	4.80	12.28	0.75
	Time (s)	4800	4800	3900	3700	4100
Temp. (19 °C)	Max. temp. (°C)	22.65	24.93	37.92	33.84	25.40
	Max. temp. difference (°C)	0.22	0.20	4.84	12.40	0.76
	Time (s)	4700	5100	3900	5000	3800
Temp. (18 °C)	Max. temp. (°C)	21.69	23.99	36.99	33.02	24.47
	Max. temp. difference (°C)	0.22	0.20	4.86	12.55	0.77
	Time (s)	4700	5100	3900	5000	3800
Temp. (17 °C)	Max. temp. (°C)	20.73	23.03	36.04	32.24	23.54
	Max. temp. difference (°C)	0.23	0.21	4.88	12.74	0.78
	Time (s)	6300	6700	5100	3300	4900

5. Performance Evaluation of Battery Pack Thermal Management

5.1. Evaluation System Establishment

In this paper, the ANP (analytic network process) and SD (system dynamics) are used to evaluate the thermal management performance of the design solution. For the evaluation of the advantages and disadvantages of the thermal management system of the lithium battery pack, the following factors were considered: good temperature control performance, management ease, economy, and safety. As these thermal management technologies have been solved in terms of safety, this factor was regarded as the cost of capital investment. Through the investigation of the lithium-ion vehicle battery pack heat event and the above analysis of the thermal management system design performance, the nine factors related to the evaluation of the thermal management system performance were determined from the three aspects of the battery pack temperature control performance, management ease, and economy, and the ANP model was constructed for the evaluation of the performance of the thermal management system of the lithium battery pack, as shown in Figure 8.

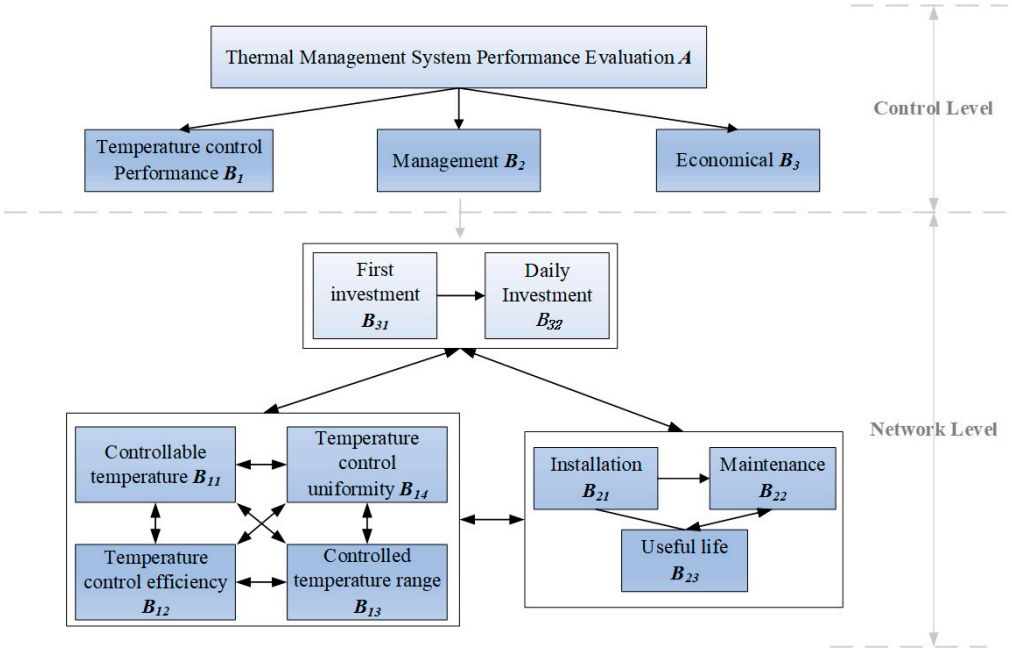

Figure 8. ANP model for thermal management system performance evaluation.

In this paper, Yaahp software was selected to solve the judgment matrix, which has the function of the automatic correction of an inconsistent judgment matrix and can consider

the psychological factors in people's decision-making, retain the expert decision data to the maximum extent, and correct the judgment matrix to meet the consistency ratio. For the established ANP model for evaluating the performance of the Li-ion battery pack thermal management system, the judgment matrix, among the elements, was constructed by choosing the 1–9 scale method according to the importance rating of experts.

The eigenvectors of each matrix were calculated using the eigen root method to obtain the weight matrix and interelement super matrix of the control layer elements and then the limit super matrix, and finally, the subjective weights of each element were obtained using the eigen root algorithm. For the established judgment matrix, the unweighted super matrix was obtained using the power method, and then each vector in the unweighted super matrix was normalized to obtain the weighted super matrix, which was normalized to obtain the limit matrix, that is, the corresponding weights of each index. The global weights of each evaluation index are shown in Table 8.

Table 8. Weighting and ranking of factors.

Control-L		**B_1**				**B_2**			**B_3**
Weighting		0.5499				0.2402			0.2098
Ranking		1				2			3
Network-L	**B_{11}**	**B_{12}**	**B_{13}**	**B_{14}**	**B_{21}**	**B_{22}**	**B_{23}**	**B_{31}**	**B_{32}**
Weighting	0.2391	0.0845	0.0409	0.1855	0.0274	0.1155	0.0974	0.1399	0.0699
Ranking	1	6	8	2	9	4	5	3	7

5.2. Construction and Simulation of System Dynamics Model

Through the construction of the performance evaluation system of the lithium battery pack thermal management system and the solution of the weights, the weight table of different influencing factors was obtained, but some elements were dynamic, such as the comprehensive controllability of temperature, temperature control efficiency, temperature control range, and the uniformity of temperature control. For this reason, a dynamic model of the thermal management system of the Li-ion battery pack was established using AnyLogic software, and the system dynamics flow diagram is shown in Figure 9, with the temperature set as stock; the integrated controllability, temperature control efficiency, temperature control range, and temperature control uniformity set as variables that change over time; and the remaining elements that do not change due to them, such as installation and maintenance, and capital investment, set as constants.

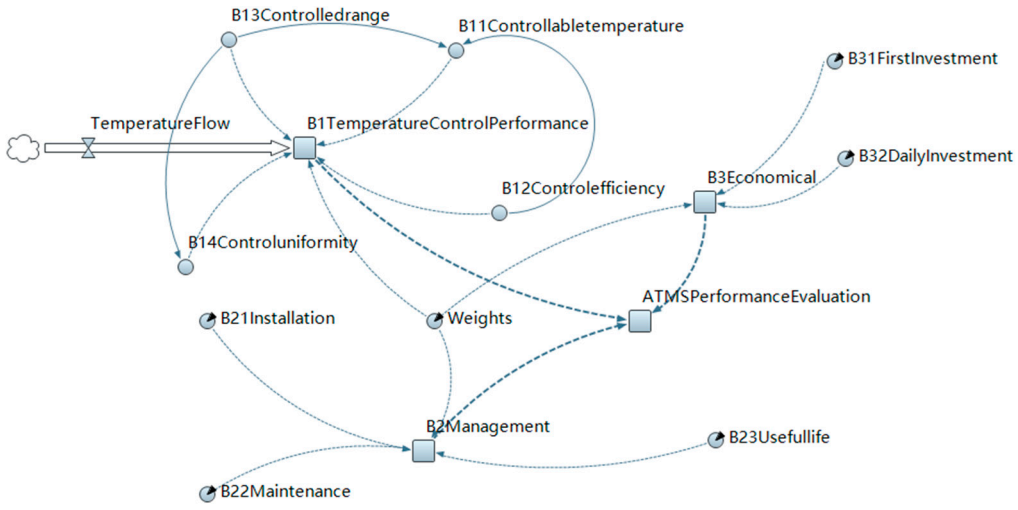

Figure 9. System dynamics flow diagram.

The following table of scoring parameters for each factor was developed with reference to the relevant technical documents of the NCM battery pack and other thermal control studies (Table 9), and a reference table of thermal management system performance scoring was developed based on the final score (Table 10). Among them, B_{11} is the rating of the maximum temperature rise of the battery pack in each model; B_{12} is the rating of how fast the battery pack reaches the maximum temperature rise; the controlled temperature range controllability B_{13} is the smoothness after reaching the temperature control requirement, and B_{14} is the rating of the temperature difference between the battery packs. According to the real situation of current battery enterprise productivity, the scores of different elements included in B_2 installation and maintenance and B_3 capital investment were obtained using expert scoring.

Table 9. Table of parameters of each factor with values.

Controllable temp. **B_{11}**	Criteria	0~25 °C	25~30 °C	30~40 °C	40~50 °C	>50 °C
	Score	100~85	85~65	65~35	35~10	<10
Temp. control efficiency **B_{12}**	Criteria	0~4000 s	4000~5000 s	5000~6000 s	6000~7000 s	>7000 s
	Score	100~85	85~65	65~35	35~10	<10
Controlled temp range **B_{13}**	Criteria	Stable	Medium	General	Fluctuating	—
	Score	100~85	85~65	65~20	<20	—
Temp. control uniformity **B_{14}**	Criteria	0~1 °C	1~3 °C	3~5 °C	>5 °C	—
	Score	100~85	85~65	65~20	<20	—
Installation **B_{21}**	Criteria	Easy	Moderate	Harder	Difficult	—
	Score	100~85	85~65	65~20	<20	—
Maintenance **B_{22}**	Criteria	Easy	Moderate	Harder	Difficult	—
	Score	100~85	85~65	65~20	<20	—
Useful life **B_{23}**	Criteria	>10 years	5~10 years	3~5 years	<3 years	—
	Score	100~85	85~65	65~20	<20	—
First investment **B_{31}**	Criteria	Low	Medium	High	Expensive	—
	Score	100~85	85~65	65~20	<20	—
Daily investment **B_{32}**	Criteria	Low	Medium	High	Expensive	—
	Score	100~85	85~65	65~20	<20	—

Table 10. Thermal management system performance score grading reference.

Total Score	>85	75~85	65~75	55~65	<55
Level	***I***	***II***	***III***	***IV***	***V***

The original simulation data simulated by each liquid-cooled thermal management temperature control design in Part 4 were imported into the system dynamics model to derive the thermal management performance scores of the different design solutions under the different operating conditions, as shown in Figure 10. The scoring and rating results show that the overall performance of the liquid-cooled designs fluctuates, with the rating range for liquid-cooled ranging from 51.7095 to 89.1055 points, and the ratings are mainly focused on Level 2. The best comprehensive ratings are Model 1 (86.7075) and Model 5 (89.1055), which can reach the level of **Level *I***. Combined with the comprehensive rating grading, it is recommended that the design of the NCM battery pack thermal management system in practical applications be set up with design ratings above **Level *I***, i.e., liquid-cooled Model 1 (18~20 °C, 0.3 m/s) and Model 5 (17~18 °C, 0.1 m/s).

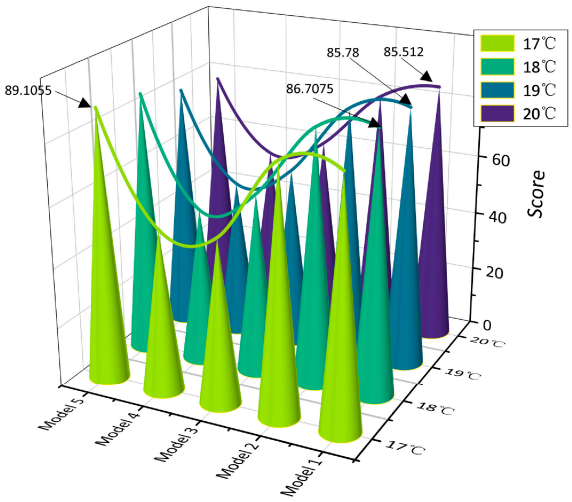

Figure 10. Performance scores for each thermal management model.

6. Conclusions

This paper investigates the heat generation and heat dissipation performance of a battery pack based on the normal heat generation and thermal runaway mechanism of lithium-ion batteries using COMSOL Multiphysics simulation platform software. For an electric vehicle NCM lithium-ion battery pack, the battery pack charging heat generation model modeling, liquid-cooled thermal management temperature control system design and simulation, and the design thermal management system performance comprehensive evaluation analysis were conducted. The main conclusions are as follows:

1. Based on the natural convection heat transfer mechanism and the Joule heat and side reaction exothermic mechanism, the high temperature of some cell singlets in the battery pack at a large charging multiplier of 0.8 C and 1 C triggers the side reaction process and develops rapidly into thermal runaway. The impact on the thermal stability of the NCM lithium-ion battery pack is great and difficult to control; the "cross"-type high-temperature area is easily formed near the center of the battery pack, which is the key area for the thermal management of the battery pack; the impact of external temperature changes on the battery exotherm is linearly superimposed;
2. The thermal management technology selects the liquid cooling method of cold plate heat exchange. Five liquid cooling temperature control models were designed purposefully, and they were simulated and analyzed for a charging multiplier under the 0.5 C working condition, flow rate working condition, and temperature working condition, respectively. The results show that (1) the initial conditions of the liquid cooling design (0.5 C, 0.1 m/s, 20 °C) have better control of the temperature difference and more uniform temperature control effect, and each model meets the requirements of the temperature control range (0~50 °C), and the maximum temperature difference between the groups of Models 1, 2, and 5 does not even exceed 1 °C; (2) the temperature control effect that can be achieved only by increasing the coolant flow rate is limited, but, in contrast, it will greatly reduce the energy utilization efficiency, and the appropriate flow rate conditions should be selected to meet the goal of economic efficiency; and (3) the effect of the coolant temperature on the temperature control effect is linearly superimposed, but changing the coolant temperature will result in more energy loss, so it should be selected appropriately in the real application;
3. Based on the ANP and SD methods, the performance of the thermal management system was comprehensively analyzed, and the evaluation system of the system performance of the thermal management scheme was established. Using this evaluation system, the system performance evaluation was scored and graded for multiple operating conditions of each thermal management model in turn. The evaluation results recommend that Model 1 and Model 5 be used in practice for the NCM battery

pack and to apply the working condition settings for which they were evaluated as Level ***I***;

4. In addition, the heat dissipation method in this paper is relatively single, and in the future, we will carry out deeper exploration based on this research, make changes in the heat dissipation method, choose a liquid cooling and phase change material coupling heat dissipation method, and carry out new research on the thermal management scheme of the lithium battery pack under the role of this heat dissipation mode.

Author Contributions: Conceptualization, methodology, formal analysis, writing—review and editing, Y.Z.; software, investigation, visualization, W.H.; writing—original draft preparation, validation, Y.Z. and W.H.; supervision, project administration, funding acquisition, J.C. All authors have read and agreed to the published version of the manuscript.

Funding: This research was funded by the National Natural Science Foundation Project of China, grant number 52274163.

Data Availability Statement: Not applicable.

Conflicts of Interest: The authors declare no conflict of interest.

References

1. Liu, S.; Liu, X.; Dou, R.; Zhou, W.; Wen, Z.; Liu, L. Experimental and Simulation Study on Thermal Characteristics of 18,650 Lithium–Iron–Phosphate Battery with and without Spot–Welding Tabs. *Appl. Therm. Eng.* **2020**, *166*, 114648. [CrossRef]
2. Bugryniec, P.J.; Davidson, J.N.; Brown, S.F. Computational Modelling of Thermal Runaway Propagation Potential in Lithium Iron Phosphate Battery Packs. *Energy Rep.* **2020**, *6*, 189–197. [CrossRef]
3. Ubale, D.; Ubale, P. A Critical Review on Recent Developments in Battery Thermal Management System of Electric Vehicles. *Mater. Today Proc.* **2022**, *68*, 2613–2621. [CrossRef]
4. Meng, J.; Yue, M.; Diallo, D. Nonlinear Extension of Battery Constrained Predictive Charging Control with Transmission of Jacobian Matrix. *Int. J. Electr. Power Energy Syst.* **2023**, *146*, 108762. [CrossRef]
5. Huang, Z.; Li, H.; Mei, W.; Zhao, C.; Sun, J.; Wang, Q. Thermal Runaway Behavior of Lithium Iron Phosphate Battery During Penetration. *Fire Technol.* **2020**, *56*, 2405–2426. [CrossRef]
6. Saw, L.H.; Somasundaram, K.; Ye, Y.; Tay, A.A.O. Electro-Thermal Analysis of Lithium Iron Phosphate Battery for Electric Vehicles. *J. Power Sources* **2014**, *249*, 231–238. [CrossRef]
7. Dong, T.; Peng, P.; Jiang, F. Numerical Modeling and Analysis of the Thermal Behavior of NCM Lithium-Ion Batteries Subjected to Very High C-Rate Discharge/Charge Operations. *Int. J. Heat Mass Transf.* **2018**, *117*, 261–272. [CrossRef]
8. Nelson, P.; Dees, D.; Amine, K.; Henriksen, G. Modeling Thermal Management of Lithium-Ion PNGV Batteries. *J. Power Sources* **2002**, *110*, 349–356. [CrossRef]
9. Kumar Thakur, A.; Sathyamurthy, R.; Velraj, R.; Saidur, R.; Pandey, A.K.; Ma, Z.; Singh, P.; Hazra, S.K.; Wafa Sharshir, S.; Prabakaran, R.; et al. A State-of-the Art Review on Advancing Battery Thermal Management Systems for Fast-Charging. *Appl. Therm. Eng.* **2023**, *226*, 120303. [CrossRef]
10. Lin, J.; Liu, X.; Li, S.; Zhang, C.; Yang, S. A Review on Recent Progress, Challenges and Perspective of Battery Thermal Management System. *Int. J. Heat Mass Transf.* **2021**, *167*, 120834. [CrossRef]
11. Kim, J.; Oh, J.; Lee, H. Review on Battery Thermal Management System for Electric Vehicles. *Appl. Therm. Eng.* **2019**, *149*, 192–212. [CrossRef]
12. Wu, W.; Wang, S.; Wu, W.; Chen, K.; Hong, S.; Lai, Y. A Critical Review of Battery Thermal Performance and Liquid Based Battery Thermal Management. *Energy Convers. Manag.* **2019**, *182*, 262–281. [CrossRef]
13. An, Z.; Jia, L.; Ding, Y.; Dang, C.; Li, X. A Review on Lithium-Ion Power Battery Thermal Management Technologies and Thermal Safety. *J. Therm. Sci.* **2017**, *26*, 391–412. [CrossRef]
14. Liu, H.; Wei, Z.; He, W.; Zhao, J. Thermal Issues about Li-Ion Batteries and Recent Progress in Battery Thermal Management Systems: A Review. *Energy Convers. Manag.* **2017**, *150*, 304–330. [CrossRef]
15. Zhang, W.; Liang, Z.; Wu, W.; Ling, G.; Ma, R. Design and Optimization of a Hybrid Battery Thermal Management System for Electric Vehicle Based on Surrogate Model. *Int. J. Heat Mass Transf.* **2021**, *174*, 121318. [CrossRef]
16. Wang, N.; Li, C.; Li, W.; Huang, M.; Qi, D. Effect Analysis on Performance Enhancement of a Novel Air Cooling Battery Thermal Management System with Spoilers. *Appl. Therm. Eng.* **2021**, *192*, 116932. [CrossRef]
17. Akinlabi, A.A.H.; Solyali, D. Configuration, Design, and Optimization of Air-Cooled Battery Thermal Management System for Electric Vehicles: A Review. *Renew. Sustain. Energy Rev.* **2020**, *125*, 109815. [CrossRef]
18. Park, H. A Design of Air Flow Configuration for Cooling Lithium Ion Battery in Hybrid Electric Vehicles. *J. Power Sources* **2013**, *239*, 30–36. [CrossRef]
19. Pesaran, A.A. Battery Thermal Models for Hybrid Vehicle Simulations. *J. Power Sources* **2002**, *110*, 377–382. [CrossRef]

20. Wang, M.; Teng, S.; Xi, H.; Li, Y. Cooling Performance Optimization of Air-Cooled Battery Thermal Management System. *Appl. Therm. Eng.* **2021**, *195*, 117242. [CrossRef]
21. Bhosale, A.J.; Deshmukh, V.N. Efficient Ways of Thermal Management of an EV Battery. *Mater. Today Proc.* **2023**, *72*, 1434–1445. [CrossRef]
22. E, J.; Han, D.; Qiu, A.; Zhu, H.; Deng, Y.; Chen, J.; Zhao, X.; Zuo, W.; Wang, H.; Chen, J.; et al. Orthogonal Experimental Design of Liquid-Cooling Structure on the Cooling Effect of a Liquid-Cooled Battery Thermal Management System. *Appl. Therm. Eng.* **2018**, *132*, 508–520. [CrossRef]
23. Chen, D.; Jiang, J.; Kim, G.-H.; Yang, C.; Pesaran, A. Comparison of Different Cooling Methods for Lithium Ion Battery Cells. *Appl. Therm. Eng.* **2016**, *94*, 846–854. [CrossRef]
24. Wu, M.-S.; Chiang, P.-C.J. High-Rate Capability of Lithium-Ion Batteries after Storing at Elevated Temperature. *Electrochim. Acta* **2007**, *52*, 3719–3725. [CrossRef]
25. Gao, R.; Fan, Z.; Liu, S. A Gradient Channel-Based Novel Design of Liquid-Cooled Battery Thermal Management System for Thermal Uniformity Improvement. *J. Energy Storage* **2022**, *48*, 104014. [CrossRef]
26. Akbarzadeh, M.; Jaguemont, J.; Kalogiannis, T.; Karimi, D.; He, J.; Jin, L.; Xie, P.; Mierlo, J.V.; Berecibar, M. A Novel Liquid Cooling Plate Concept for Thermal Management of Lithium-Ion Batteries in Electric Vehicles. *Energy Convers. Manag.* **2021**, *231*, 113862. [CrossRef]
27. Jilte, R.; Afzal, A.; Panchal, S. A Novel Battery Thermal Management System Using Nano-Enhanced Phase Change Materials. *Energy* **2021**, *219*, 119564. [CrossRef]
28. Landini, S.; Leworthy, J.; O'Donovan, T.S. A Review of Phase Change Materials for the Thermal Management and Isothermalisation of Lithium-Ion Cells. *J. Energy Storage* **2019**, *25*, 100887. [CrossRef]
29. Cheng, G.; Wang, Z.; Wang, X.; He, Y. All-Climate Thermal Management Structure for Batteries Based on Expanded Graphite/Polymer Composite Phase Change Material with a High Thermal and Electrical Conductivity. *Appl. Energy* **2022**, *322*, 119509. [CrossRef]
30. Chen, X.; Zhou, F.; Yang, W.; Gui, Y.; Zhang, Y. A Hybrid Thermal Management System with Liquid Cooling and Composite Phase Change Materials Containing Various Expanded Graphite Contents for Cylindrical Lithium-Ion Batteries. *Appl. Therm. Eng.* **2022**, *200*, 117702. [CrossRef]
31. Lin, X.; Zhang, X.; Liu, L.; Liang, J.; Liu, W. Polymer/Expanded Graphite-Based Flexible Phase Change Material with High Thermal Conductivity for Battery Thermal Management. *J. Clean. Prod.* **2022**, *331*, 130014. [CrossRef]
32. Li, W.Q.; Qu, Z.G.; He, Y.L.; Tao, Y.B. Experimental Study of a Passive Thermal Management System for High-Powered Lithium Ion Batteries Using Porous Metal Foam Saturated with Phase Change Materials. *J. Power Sources* **2014**, *255*, 9–15. [CrossRef]
33. Wang, Z.; Zhang, Z.; Jia, L.; Yang, L. Paraffin and Paraffin/Aluminum Foam Composite Phase Change Material Heat Storage Experimental Study Based on Thermal Management of Li-Ion Battery. *Appl. Therm. Eng.* **2015**, *78*, 428–436. [CrossRef]
34. Babapoor, A.; Azizi, M.; Karimi, G. Thermal Management of a Li-Ion Battery Using Carbon Fiber-PCM Composites. *Appl. Therm. Eng.* **2015**, *82*, 281–290. [CrossRef]
35. Liu, C.; Xu, D.; Weng, J.; Zhou, S.; Li, W.; Wan, Y.; Jiang, S.; Zhou, D.; Wang, J.; Huang, Q. Phase Change Materials Application in Battery Thermal Management System: A Review. *Materials* **2020**, *13*, 4622. [CrossRef]
36. Luo, X.; Guo, Q.; Li, X.; Tao, Z.; Lei, S.; Liu, J.; Kang, L.; Zheng, D.; Liu, Z. Experimental Investigation on a Novel Phase Change Material Composites Coupled with Graphite Film Used for Thermal Management of Lithium-Ion Batteries. *Renew. Energy* **2020**, *145*, 2046–2055. [CrossRef]
37. Yang, K.; Ling, Z.; Fang, X.; Zhang, Z. Introducing a Flexible Insulation Network to the Expanded Graphite-Based Composite Phase Change Material to Enhance Dielectric and Mechanical Properties for Battery Thermal Management. *J. Energy Storage* **2023**, *66*, 107486. [CrossRef]
38. Xie, L.; Huang, Y.; Lai, H. Coupled Prediction Model of Liquid-Cooling Based Thermal Management System for Cylindrical Lithium-Ion Module. *Appl. Therm. Eng.* **2020**, *178*, 115599. [CrossRef]
39. Ji, C.; Wang, B.; Wang, S.; Pan, S.; Wang, D.; Qi, P.; Zhang, K. Optimization on Uniformity of Lithium-Ion Cylindrical Battery Module by Different Arrangement Strategy. *Appl. Therm. Eng.* **2019**, *157*, 113683. [CrossRef]
40. Wang, B.; Ji, C.; Wang, S.; Sun, J.; Pan, S.; Wang, D.; Liang, C. Study of Non-Uniform Temperature and Discharging Distribution for Lithium Ion Battery Modules in Series and Parallel Connection. *Appl. Therm. Eng.* **2020**, *168*, 114831. [CrossRef]
41. Choudhari, V.G.; Dhoble, A.S.; Sathe, T.M. A Review on Effect of Heat Generation and Various Thermal Management Systems for Lithium Ion Battery Used for Electric Vehicle. *J. Energy Storage* **2020**, *32*, 101729. [CrossRef]
42. Fan, L.; Khodadadi, J.M.; Pesaran, A.A. A Parametric Study on Thermal Management of an Air-Cooled Lithium-Ion Battery Module for Plug-in Hybrid Electric Vehicles. *J. Power Sources* **2013**, *238*, 301–312. [CrossRef]
43. Khateeb, S.A.; Farid, M.M.; Selman, J.R.; Al-Hallaj, S. Design and Simulation of a Lithium-Ion Battery with a Phase Change Material Thermal Management System for an Electric Scooter. *J. Power Sources* **2004**, *128*, 292–307. [CrossRef]